Recombinant Toluene-4-monooxygenase: Catalytic and Mössbauer Studies of the Purified Diiron and Rieske Components of a Four-Protein Complex†

Jeremie D. Pikus,‡ Joey M. Studts,‡ Catalina Achim,§ Karl E. Kauffmann,§ Eckard Münck,§ Robert J. Steffan,|| Kevin McClay,|| and Brian G. Fox*,‡

The Institute for Enzyme Research, Graduate School and Department of Biochemistry, College of Agricultural and Life Sciences, University of Wisconsin, Madison, Wisconsin 53705, Department of Chemistry, Carnegie Mellon University, Pittsburgh, Pennsylvania 15213, and Envirogen, Lawrenceville, New Jersey 08648

Received February 26, 1996; Revised Manuscript Received May 9, 1996⊗

ABSTRACT: Expression of the *tmoA-F* gene cluster from *Pseudomonas mendocina* KR1 in *Escherichia coli* BL21(DE3) produces a catalytically active form of the toluene-4-monooxygenase (T4MO) complex. Here we report the purification and characterization of four soluble proteins required for the *in vitro* reconstitution of T4MO catalytic activity. These proteins are a diiron hydroxylase (T4MOH), a Rieske-type ferredoxin (T4MOC), an effector protein (T4MOD), and an NADH oxidoreductase (T4MOF). The T4MOH component is composed of the *tmoA*, *tmoB*, and *tmoE* gene products [quaternary structure $(\alpha\beta\epsilon)_2$, $M_r \approx 220$ kDa]. The T4MOA polypeptide contains two copies of the amino acid sequence motif (D/E)$X_{(28-37)}$DEXRH; the same motif provides all of the protein-derived ligands to the diiron centers of ribonucleotide reductase, the soluble methane monooxygenase, and the stearoyl-ACP Δ^9 desaturase. Mössbauer, optical, and EPR measurements show that the T4MOH contains diiron centers and suggest that the diiron center contains hydroxo bridge(s) in the diferric state, as observed for methane monooxygenase. Mössbauer and EPR measurements also show that the T4MOC contains a Rieske-type iron−sulfur center. This assignment is in accord with the presence of the amino acid sequence motif $CPHX_{(15-17)}CX_2H$, which has also been found in the bacterial, chloroplastic, and mitochondrial Rieske proteins as well as the bacterial NADH-dependent *cis*-dihydrodiol-forming aromatic dioxygenases. While single-turnover catalytic studies confirm the function of the T4MOH as the hydroxylase, the NADH-dependent multiple-turnover hydroxylation activity is increased by more than 100-fold in the presence of the T4MOC, which mediates highly specific electron transfer between the T4MOF and the T4MOH. The T4MOD can be purified as an 11.6 kDa monomeric protein devoid of cofactors or redox-active metal ions; this component is also detected as a substoichiometric consitutent of the purified T4MOH. The rate of the hydroxylation reaction can be mildly stimulated by the further addition of separately purified T4MOD to the T4MOH, implying the formation of a high affinity, catalytically competent complex between these two components. These characterizations define a novel, four-component oxygenase combining elements from the soluble methane oxidation complex of the methanotrophic bacteria and the aromatic hydroxylation complexes of the soil pseudomonads.

The aerobic, bacterial oxidation of toluene is catalyzed by five distinct multicomponent complexes, whose products are shown in Figure 1. The presently available biochemical and structural properties indicate that these complexes contain three types of structurally distinct active sites. One of these complexes, the toluene dioxygenase from *Pseudomonas putida* F1 (TDO,[1] Figure 1A), catalyzes the NADH- and O_2-dependent dioxygenation of toluene, forming a *cis*-dihydrodiol (Gibson et al., 1970). The active site of TDO contains both a Rieske-type [2Fe-2S] center and a mononuclear iron center (Mason & Cammack, 1992).

A second, structurally less well defined active site used for the oxidation of toluene is found in xylene monooxygenase (Suzuki et al., 1991), which catalyzes the monooxygenation of the methyl substituent of toluene and xylenes (Figure 1B). Xylene monooxygenase is a member of a proposed family of iron-containing integral membrane proteins (Shanklin et al., 1994) that includes the alkane hydroxylase from *Pseudomonas oleovorans* and the eukaryotic fatty acid desaturases. All members of this family

† This work was supported by grants from the Institute for Enzyme Research, Graduate School, and the Department of Biochemistry, College of Agricultural and Life Sciences, University of Wisconsin, the Petroleum Research Foundation (ACS-PRF 28405-G4), the NIH (GM-50853 to B.G.F. and GM-22701 to E.M.), and the NSF Small Business Innovation Research Program (DMI-9460076 to R.J.S.). B.G.F. is a Searle Scholar of the Chicago Community Trust (1994−1997) and a Shaw Scientist of the Milwaukee Foundation (1994−1999).

* Author to whom correspondence should be addressed.

‡ The Institute for Enzyme Research.

§ Carnegie Mellon University.

|| Envirogen.

⊗ Abstract published in *Advance ACS Abstracts,* June 15, 1996.

[1] Abbreviations: MOPS, 3-(*N*-morpholino)propanesulfonic acid; MMO, methane monooxygenase; T2MO, toluene-2-monooxygenase; T3MO; toluene-3-monooxygenase; T4MO, toluene-4-monooxygenase; T4MOH, the hydroxylase component of the T4MO; T4MOA, 55 kDa subunit of the T4MOH, the product of the *tmoA* gene; T4MOB, 9.6 kDa subunit of the T4MOH, the product of the *tmoB* gene; T4MOC, 12.5 kDa Rieske-type ferredoxin, the product of the *tmoC* gene; T4MOD, 11.6 kDa product of the *tmoD* gene; T4MOE, 35 kDa subunit of the T4MOH, the product of the *tmoE* gene; T4MOF, reductase component of T4MO, the product of the *tmoF* gene; TDO, toluene dioxygenase.

S0006-2960(96)00456-4 CCC: $12.00

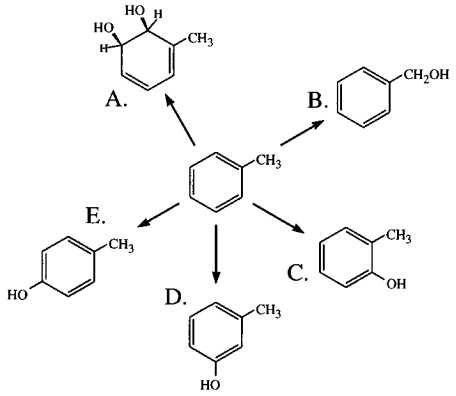

FIGURE 1: Diversity of bacterial pathways used for the NAD(P)H- and O_2-dependent oxidation of toluene. (A) Toluene dioxygenase from *Pseudomonas putida* F1 (Wackett, 1990); (B) xylene monooxygenase from *P. putida* mt-2 (Suzuki et al., 1991); (C) toluene-2-monooxygenase from *Burkholderia cepacia* G4 (Shields et al., 1995); (D) toluene-3-monooxygenase from *P. pickettii* PKO1 (Olsen et al., 1994); (E) toluene-4-monooxygenase from *P. mendocina* KR1 (Whited & Gibson, 1991).

contain a total of eight identically conserved His residues. Site-directed mutagenic studies of the rat stearoyl-CoA Δ^9 desaturase (Shanklin et al., 1994) have shown that these His residues are required for catalytic function, possibly serving as ligands for the iron atom(s) present in the catalytic center.

On the basis of our identification of two copies of the amino acid sequence motif (D/E)$X_{(\sim 30)}$DEXRH in the toluene-4-monooxygenase from *Pseudomonas mendocina* KR1 (T4MO, Figure 1E), we proposed that the T4MO would contain a diiron center: a third type of catalytic active site used for the oxidation of toluene (Fox et al., 1994). The T4MO enzyme complex has the ability to oxidize heterocyclic aromatic compounds such as indole and halogenated solvents such as trichloroethylene and chloroform (McClay et al., 1996), which has contributed to our interest in this enzyme (McClay et al., 1995). As part of our studies of the catalytic and structural properties of the T4MO, we have purified the hydroxylase (T4MOH) and ferredoxin (T4MOC) components of the complex from cell extracts of an *Escherichia coli* expression host and report their spectroscopic and catalytic characterization. In addition, we report that *two* other protein components participate in the *in vitro* T4MO catalytic turnover, namely, an 11.6 kDa effector protein (T4MOD) and an NADH oxidoreductase (T4MOF). These efforts define a new type of multicomponent oxygenase combining structural and functional elements from both the aromatic hydroxylation complexes of the soil pseudomonads and the soluble MMO of the methanotrophic bacteria. The presence of protein elements previously associated with only the MMO complex provides further evidence for the existence of a protein family of evolutionarily related soluble bacterial diiron hydroxylases.

MATERIALS AND METHODS

Construction of Expression Vectors. The steps used to construct the expression vectors pRS184 and pRS202 are summarized in Figure 2. The *tmoA-F* gene cluster is contained on a contiguous 4.7 kb region of *P. mendocina* KR1 chromosomal DNA (Yen & Karl, 1992) and was isolated as previously described (Wilson, 1993). The

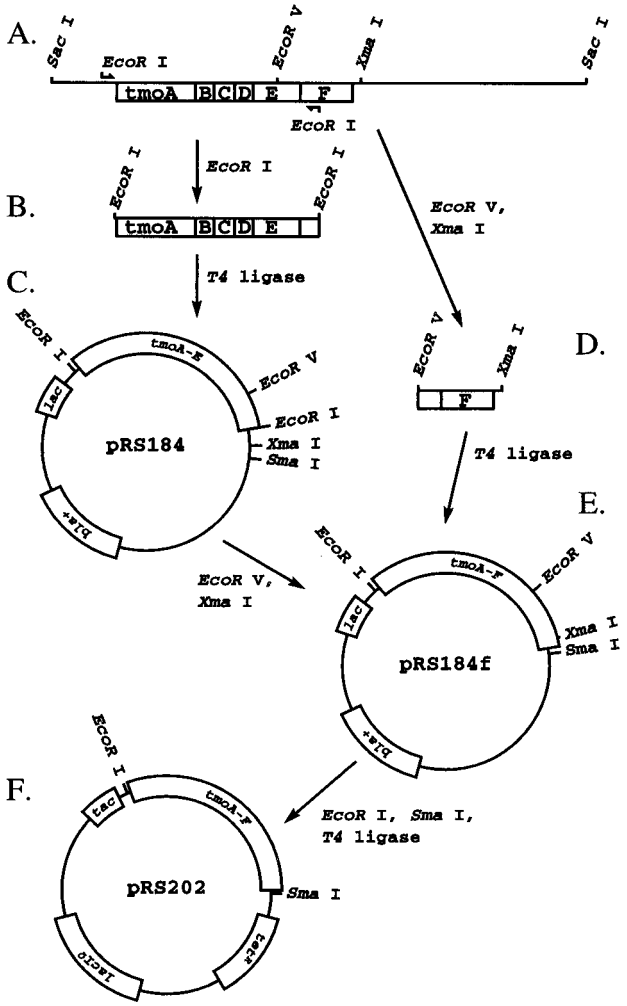

FIGURE 2: Summary of the assembly of the expression vectors pRS184 and pRS202 from *P. mendocina* KR1 chromosomal DNA containing the *tmoA-F* gene cluster.

catabolic genes *tmoA-E* were amplified by polymerase chain reaction from the genomic DNA using the primers TMOU1 (5′-CGGAATTCTTTAAACCCCACAGGCACGG) and TCED3 (5′-GCGAATTCGATAATGGTTTGCACTGCCA), which incorporated *Eco*RI restriction sites into each end of the 3652 bp amplified fragment (Figure 2A). Polymerase chain reaction was performed using a GeneAmp kit and the reaction conditions recommended by the manufacturer (Perkin Elmer, Foster City, CA). Cycling conditions were as follows: 1 min at 94 °C; 30 s at 50 °C; and 3 min at 71 °C for 25 cycles, followed by a 71 °C incubation for 7 min. The amplified DNA fragment was digested with *Eco*RI (Figure 2B) using conditions recommended by the enzyme supplier (New England Biolabs, Inc., Beverly, MA), ligated to similarly digested pUC18Not (Herrero et al., 1990), and used to transform *E. coli* JM109. Positive clones were selected by plating onto Luria Bertani medium agar plates containing 100 μg/mL ampicillin, followed by replica plating onto plates containing ampicillin, 100 μg/mL indole, and 20 μg/mL IPTG. Colonies that formed a blue color, resulting from the T4MO-catalyzed oxidation of indole leading to indigo formation, were selected for further analysis by restriction mapping. A plasmid containing the correct 3642 bp insert was selected and named pRS184 (Figure 2C). Plasmid pRS184 was maintained in *E. coli* DH5α on Luria Bertani medium supplemented with 100 μg/mL ampicillin.

To clone the *tmoA-F* gene cluster, total genomic DNA from *P. mendocina* KR1 was digested with *Eco*RV and *Xma*I and separated by agarose gel electrophoresis (Figure 2D). Fragments ranging from 2 to 3 kb were ligated to similarly digested pRS184 and used to transform *E. coli* DH5α (Gibco BRL, Gaithersburg, MD). Positive clones were selected for their ability to convert indole to indigo as described above. Restriction analysis was used to confirm that positive clones contained an insert corresponding to the size of the *tmoA-F* gene cluster (pRS184f, Figure 2E). The plasmid pRS184f was then digested with *Eco*RI and *Sma*I, the 4727 bp fragment was purified by agarose gel electrophoresis, and the fragment was ligated into similarly digested and purified pVLT31 (De Lorenzo et al., 1993). The ligation mixture was used to transform *E. coli* BL21 (DE3) (Novagen, Inc. Madison, WI). Clones were selected by growth on Luria Bertani medium agar plates containing 10 μg/mL tetracycline, followed by screening for catalytic function on plates containing tetracycline, indole, and IPTG. A plasmid containing the correct insert was selected and the clone used during this work was designated pRS202 (Figure 2F). Plasmid pRS202 was maintained in *E. coli* BL21(DE3) on Luria Bertani medium supplemented with 5 μg/mL tetracycline.

Expression of T4MO. For expression of the T4MO complex from pRS202, the expression host was grown in a fermenter (14 L working volume) in a complex medium supplemented with 5 μg/mL tetracycline (Hoffman et al., 1995). The fermenter was inoculated with a 5% (v/v) starting inoculum having an optical density at 600 nm of ∼1, and the culture was allowed to grow at 37 °C until the optical density was ∼4.0. Gene expression was induced by the addition of isopropyl β-D-galactopyranoside (0.05 mM), and the temperature was adjusted to 25 °C. At the time of induction, 2 mL per L of an iron-containing solution (1.12 g of $FeSO_4 \cdot 7H_2O$ dissolved in 95 mL of deionized water acidified with 5 mL of 0.25 M H_2SO_4) was added to the fermentation medium. After 5 h, the cells were harvested and washed with 25 mM phosphate buffer, pH 7.0, by using a tangential-flow membrane concentrator. The cell paste was stored at −80 °C. A typical cell yield was 5−8 g of wet cell paste per liter of culture medium. For preparation of the ^{57}Fe-enriched proteins, ^{57}Fe metal (95.5% isotopic enrichment, Advanced Materials Technology) was dissolved in a minimal volume of concentrated HCl and added to the fermentation medium at the time of induction. After the addition of ^{57}Fe, an isotopic enrichment of ∼70% was achieved in the fermenter medium.

Separation of T4MO into Three Fractions. Unless otherwise noted, all purification buffers were prepared from distilled and deionized water, and all purification procedures were carried out at 4 °C. The cell paste (∼150 g) was placed in a 500-mL stainless steel beaker suspended in a 60 °C water bath and thawed rapidly by stirring. The cell paste was then suspended in 150 mL of 25 mM MOPS, pH 6.9, containing 100 μM $Fe(NH_4)_2(SO_4)_2$, 2 mM cysteine, 1% (v/v) glycerol, and 10% (v/v) ethanol (buffer A). Lysozyme, DNAse, and RNAse (1 mg of each) were added to the cell suspension, and the cell suspension was gently stirred for 5 min at 4 °C. The cell suspension was sonicated for a total of 14 min. During the sonication, the temperature of the cell suspension was maintained below 7 °C by placing the stainless steel beaker in an ice bath and by stopping the sonication. The sonicated cell suspension was centrifuged at 39200*g* for 60 min. The supernatant was decanted and diluted with two volumes of buffer A. This preparation, called the cell-free extract, was loaded onto a Fast Flow DEAE-Sepharose CL-6B column (45 × 250 mm) equilibrated in buffer A at a linear flow rate of 40 cm/h. After loading, the column was washed with ∼500 mL of buffer A containing 0.08 M NaCl. All T4MO components were adsorbed under these conditions. Following the wash, a 1.2 L linear gradient of 0.08−0.45 M NaCl in buffer A was applied at a linear flow rate of 18 cm/h. Fractions containing the T4MOF (reductase) were identified by use of a gas chromatographic assay for the production of *p*-cresol described below and eluted at ∼0.2 M NaCl. Fractions containing the T4MOD not tightly bound to the T4MOH were pooled on the basis of visual examination of denaturing polyacrylamide gels and eluted at ∼0.22 M NaCl. Fractions containing the T4MOH (hydroxylase) were identified upon the basis of a gas chromatographic assay for the production of *p*-cresol described below and eluted at ∼0.35 M NaCl. Fractions of the T4MOH were also examined by denaturing polyacrylamide gel electrophoresis and were pooled on the basis of both catalytic activity and visual examination of the denaturing gels. Fractions of the T4MOC were identified by optical spectroscopy and eluted at ∼0.45 M NaCl.

Further Purification of T4MOD and T4MOF. Fractions containing T4MOD and T4MOF were pooled together, brought to 100 mM MOPS, pH 7.5, by the addition of 1 M MOPS, pH 7.5, and adjusted to contain 1 mM mercaptoacetic acid. The T4MOD and T4MOF were precipitated by addition of $(NH_4)_2SO_4$ to 50% of saturation at 4 °C. After slowly stirring for 1 h, the precipitate was recovered by centrifugation at 39200*g* for 15 min. The pellets were redissolved in a minimal volume (20−30 mL) of 25 mM MOPS, pH 7.5, containing 50 mM NaCl and 1 mM mercaptoacetic acid (buffer B). A slight amount of insoluble protein was removed by centrifugation at 32900*g* for 15 min. The clarified T4MOD and T4MOF solution was loaded onto a Sephacryl S-100 column (40 × 1000 mm) equilibrated in buffer B and eluted at a linear flow rate of 1.5 cm/h. The T4MOD and T4MOF were completely resolved by this chromatographic step, and purified T4MOD (∼10−20 mg) was obtained as judged by denaturing gel electrophoresis. The purified T4MOD was concentrated by ultrafiltration (YM3), frozen in liquid nitrogen, and stored at −80 °C. Fractions of T4MOF from the Sephacryl S-100 column were identified as described above and consisted of ∼50% of a polypeptide with $M_r \approx 36$ kDa, as estimated by denaturing gel electrophoresis. These fractions were concentrated by ultrafiltration (YM30), frozen in liquid nitrogen, and stored at −80 °C.

Further Purification of the T4MOH. The pooled T4MOH was concentrated using ultrafiltration (YM100, 20−30 mL, ∼80 mg/mL), centrifuged at 39200*g* for 15 min to remove a minor amount of particulate material, and applied to a Sephacryl S-300 (40 × 1000 mm) column equilibrated in buffer A containing 0.2 M NaCl and 5% (v/v) glycerol, and eluted at a linear flow rate of 3 cm/h. Fractions containing the T4MOH were identified and pooled as described above. The pooled T4MOH was diluted with an equal volume of 25 mM MOPS, pH 6.9, containing 5% (v/v) glycerol (buffer C), and was loaded onto a MonoQ 26/10 FPLC column equilibrated in buffer C at a linear flow rate of 40 cm/h.

After loading, the column was washed with ~200 mL of buffer C containing 0.3 M NaCl. Following the wash, a 0.6 L linear gradient of 0.30−0.60 M NaCl in buffer C was used to elute the T4MOH at a linear flow rate of 3 cm/h. Fractions containing the T4MOH were identified as described above, pooled, concentrated using ultrafiltration, frozen in liquid nitrogen, and stored at −80 °C.

Further Purification of the T4MOC. The pooled T4MOC was diluted with three volumes of ice-cold 25 mM MOPS, pH 7.5 (buffer D), and loaded onto a Fast Flow DEAE Sepharose CL-6B column (10 × 100 mm) equilibrated in buffer D at a linear flow rate of 40 cm/h. The T4MOC was batch eluted with buffer D containing 0.8 M NaCl at a linear flow rate of 0.5 cm/h, typically in a volume of 8 mL or less. The concentrated T4MOC was applied to a Sephacryl S-100 column (40 × 500 mm) equilibrated in buffer D containing 200 mM NaCl at a linear flow rate of 3 cm/h. Fractions of the T4MOC were identified by optical spectroscopy, examined by denaturing polyacrylamide gel electrophoresis, and pooled on the basis of both optical measurements and visual examination of the denaturing gels. The purified T4MOC was concentrated using ultrafiltration, frozen in liquid nitrogen, and stored at −80 °C.

Protein Characterizations. Denaturing polyacrylamide gel electrophoresis was performed in 12% acrylamide (70 × 80 × 0.75 mm gels) using a Tris/Tricine, sodium dodecyl sulfate buffer system (Schägger & von Jagow, 1987). Protein samples were prepared for electrophoresis by incubation in denaturing sample buffer [1% (v/v) sodium dodecyl sulfate and 5 mM β-mercaptoethanol] at 95 °C for 5 min prior to electrophoresis. Native molecular weights were determined by gel filtration in a Sephacryl S-300 26/60 FLPC column equilibrated in 25 mM MOPS buffer, pH 7.0, containing 50 mM NaCl. The molecular weight markers (Sigma, Saint Louis, MO) used as standards for gel filtration chromatography were (substance, kDa): blue dextran, 2000; ferritin, 443; catalase, 248; aldolase, 160; hemoglobin, 64.5; lysozyme, 14.4. Protein concentrations were determined colorimetrically as previously described (Fox et al., 1989). Amino-terminal sequencing was performed at the University of Wisconsin Biotechnology Center Microsequencing Facility on polypeptides separated by denaturing gel electrophoresis and then electroblotted onto polyvinylidene difluoride membranes (Matsudaira, 1987). Total iron content was determined colorimetrically by complexation with tripyridyl-*S*-triazine (Fischer & Price, 1964). Total metal content was determined at the University of Wisconsin Extension Soil and Plant Analysis Laboratory by inductively coupled plasma emission spectrometry.

Spectroscopic Methods. Optical spectra were obtained on a Hewlett Packard 8452 diode array spectrophotometer. EPR spectra of the reduced T4MOH were recorded at X-band (9.34 GHz) using a Bruker ESP 300 spectrometer, a Bruker ESR 910 liquid He cryostat, and a Bruker ER 4116 DM dual mode cavity. EPR spectra of the T4MOC were recorded at X-band (9.2 GHz) using a Varian E-Line spectrometer interfaced with an IBM-AT microcomputer for data acquisition, Varian E-102 microwave bridge, Oxford Instruments ESR 900 continuous-flow liquid He cryostat, and Oxford Instruments 3120 temperature controller. Mössbauer spectra were obtained and analyzed as previously described (Fox et al., 1993a). Spectral simulations were generated using the WMOSS software package (WEB Research, Edina, MN). Reduced samples of the T4MOH were produced by the anaerobic addition of a 2-fold molar excess of sodium dithionite relative to the concentration of metal centers in the presence of the redox mediator methyl viologen (50 μM); reduced T4MOC was produced by the same procedure without the addition of methyl viologen. Sodium dithionite was prepared as a 100 mM solution in 100 mM MOPS, pH 7.0, in a teflon-sealed reaction vial. Further manipulations of the reduced EPR and Mössbauer samples were as previously described (Fox et al., 1989).

Catalytic Assay of the Reconstituted T4MO Complex. The production of *p*-cresol was measured using a Hewlett Packard 5830A gas chromatograph equipped with an 18835B capillary inlet system and an Econo-Cap SE-30 column (15 m × 0.53 mm, 1.2 μm film thickness, Alltech Associates, Deerfield IL). The column was maintained isothermally at 150 °C, the injection port was maintained at 250 °C, and the flame ionization detector was maintained at 300 °C. Helium carrier gas flow was ~3 mL/min. For these conditions, the following approximate elution times were observed: toluene, 1.2 min; decane, 1.9 min; *p*-cresol, 2.2 min.

Single-turnover assays of the individual components (100 nmol aliquots of T4MOH, T4MOC, and T4MOD) and each possible combination of these three components were performed in teflon-sealed 3 mL screw-capped reaction vials in a total buffer volume of 250 μL. The reaction buffer was 25 mM phosphate, pH 7.5, containing 50 μM methyl viologen as a redox mediator. The reaction mixture was made anaerobic by repeated cycles of flushing and filling with O_2-free Ar gas. A 2-fold molar excess of sodium dithionite relative to the concentration of metal centers was added using a gas-tight syringe. Toluene (0.5 μL, ~5 μmol) was added, and the reaction vial was incubated for 3 min. The single-turnover reaction was initiated by injection of air (3 mL) into the reaction vial. After vigorous mixing by shaking, the reaction mixture was quenched by the rapid injection into an extraction mixture containing 250 μL of 0.1 M HCl saturated with NaCl, and 500 μL of $CHCl_3$ containing 25 μM decane as an internal quantitation standard. The quenched reaction mixture was vortexed for 20 s, and the aqueous and organic layers were allowed to separate by standing. The organic layer was then removed and further clarified by centrifugation at 16000*g* for 3 min. A 2 μL sample was analyzed by gas chromatography as described above with a split ratio of ~30:1.

Multiple-turnover assays for the production of *p*-cresol were performed in teflon-sealed, 5 mL crimp-top reaction vials containing a total buffer volume of 250 μL. The reaction buffer was 50 mM phosphate, pH 7.5. Toluene (2 μL, ~20 μmol) was added by gas-tight syringe, and the reaction was initiated by the addition of NADH (0.25 μmol, to provide an initial concentration of 1 mM in the reaction vial). Aliquots (50 μL) of the reaction mixture were withdrawn at appropriate time points, quenched by the sequential addition of 50 μL of 0.1 M HCl saturated with NaCl, and 100 μL of $CHCl_3$ containing 25 μM decane as an internal quantitation standard. Subsequent manipulations were as described above for single-turnover assays. In the presence of optimal amounts of the T4MOC, T4MOD, and T4MOF, a 250 μL reaction volume containing 10 μM T4MOH produced sufficient levels of *p*-cresol (10−1000 μM) to serve as the standard assay for reconstitution of the enzyme activity. A strategy similar to that previously

Table 1: Summary of the Purification of Recombinant Toluene-4-monooxygenase[a]

step	volume (mL)	total protein (mg)	total activity (milliunits)[b]	specific activity (milliunits/mg)	yield (%)	purification (-fold)
T4MOH						
cell-free extract	176	16 300	288 600	17	100	1
DEAE Sepharose	159	3500	186 000	53	64	3
Sephacryl S-300	118	1200	142 800	118	49	7
Mono-Q	60	420	108 000	257	37	15
T4MOC						
cell-free extract	170	15 830	1 203 000	76	100	1
DEAE Sepharose	135	216	661 500	3 100	55	40
Sephacryl S-100	58	63	377 000	6 020	31	79
Mono-Q	47	23	329 600	14 270	27	188
T4MOF[c]						
cell-free extract	380	13 072	5 814 000	444	100	1
DEAE Sepharose	250	2 500	4 697 000	3 681	81	8
Sephacryl S-100	81	113	2 709 450	23 892	47	54

[a] The results reported for each component were obtained from different purification trials. [b] A unit is defined as the production of 1 μmol of *p*-cresol/min under standard assay conditions. [c] This protocol provides T4MOF with ~50% purity as determined by denaturing gel electrophoresis.

developed for the MMO was used to determine the optimal amounts of each T4MO component required in the assays (Fox et al., 1990).

RESULTS

Expression of T4MO in E. coli. Cultures of *E. coli* DH5α containing pRS184 produced a functional T4MO complex as judged by the ability of induced whole cells to convert indole to indigo and by the ability of both whole cells and cell free extracts to catalyze the oxidation of toluene to *p*-cresol. Several preliminary studies were undertaken using cell-free extracts prepared from this host strain, including the development of partial purification protocols and preliminary spectroscopic characterizations (Fox et al., 1994). However, despite these promising initial results, two factors limited our interest in the long-term use of the pRS184 expression plasmid. First, a considerable level of read-through expression was observed from this high-copy number plasmid in *E. coli* DH5α, which only produces constitutive levels of the *lac* repressor. Since T4MO is capable of the adventitious NADH- and O_2-dependent oxidation of a number of compounds, the unregulated expression was judged to contribute to the marked instability of the expression host during fermentation scale-up. Second, the cloning strategy used to produce pRS184 did not provide the complete coding region of the *tmoF* gene. In accord with previous observations (Yen et al., 1991), the *in vivo* catalytic activity observed upon expression from pRS184 was likely dependent on the adventitious participation of host strain reductases in the electron transfer reactions required for T4MO catalysis. However, attempts to reconstitute the T4MO activity using column fractions obtained from the ion exchange chromatographic separation of pRS184-derived cell-free extracts were unsuccessful.

For the above-mentioned reasons, we constructed an alternative expression vector that explicitly contained the complete coding region for *tmoA-F* (pRS202, see Figure 2). This vector is derived from the plasmid pVLT31, a low-copy number plasmid providing a multicloning site immediately adjacent to the *tac* promoter, the constitutive expression of the *lac* repressor, selection via tetracycline resistance, and broad host range compatibility (De Lorenzo et al., 1993). We have found that pRS202 can be reliably maintained in *E. coli* BL21(DE3) during bench-scale fermentations in the presence of 5 μM tetracycline. The host strain BL21(DE3) was selected to facilitate later development of expression procedures using chemically defined minimal media (Hoffman et al., 1995). No modifications of the promotor region of the plasmid pVLT31 were undertaken in these studies. Thus, it is most likely that the inducible expression proceeded via normal functioning of the *tac* promotor with *E. coli* RNA polymerase, as opposed to the action of the T7 RNA polymerase also present in this particular host. Scanning densitometric analysis of denaturing polyacrylamide gels showed that the T4MOA ($M_r \approx 55$ kDa) and T4MOE ($M_r \approx 35$ kDa) polypeptides accounted for ~5−10% of the total cellular protein at maximal induction, representing only 30% of the expression level relative to that observed from the high-copy number pRS184 expression vector. However, the pRS202 expression vector provided a roughly 10-fold increase in the toluene hydroxylation activity of cell free extracts relative to that obtained from pRS184. Our development of purification protocols was facilitated by the ability to reconstitute enzymatic activity *in vitro*, which was likely due to the functional expression of the T4MOF provided by this construct and to the higher specific activity of the T4MOH produced from lower level expression in the pVLT31 expression system.

Purification of the T4MO Components. A summary of the protocols which provide purified preparations of the hydroxylase (T4MOH) and ferredoxin (T4MOC) components and a partially purified preparation of the reductase (T4MOF) component of the T4MO complex are shown in Table 1. A denaturing electrophoretic gel containing the purified T4MOH, effector protein (T4MOD), and T4MOC components is shown in Figure 3.

Figure 3, lane 2, shows that purified preparations of T4MOH contain two large polypeptides [T4MOA ($M_r \approx 55$ kDa); T4MOE ($M_r \approx 35$ kDa)] and two smaller polypeptides. The T4MOA and T4MOE subunits were identified by comparison to the sizes predicted from the gene sequences. These assignments are supported by the work of Yen et al. (1991), who electroeluted overexpressed T4MO polypeptides from denaturing gels containing partially purified proteins (but not assayed for catalytic function) and performed

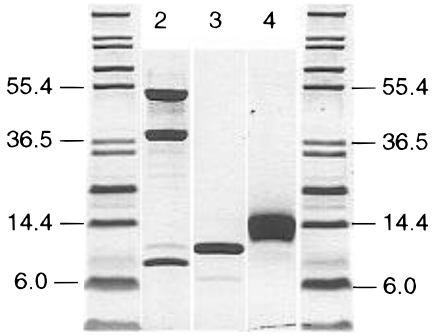

FIGURE 3: Denaturing polyacrylamide gel electrophoretic analysis of protein components of the T4MO enzyme complex. Lanes 1 and 5, molecular weight standards; lane 2, T4MOH (15 μg total protein); lane 3, T4MOD, (10 μg total protein); lane 4, T4MOC (15 μg total protein). The protein molecular weight markers (Novex, San Diego, CA) used for denaturing gel electrophoresis were (protein, kDa): rabbit muscle myosin, 200; β-galactosidase, 116.3; phosphorylase *b*, 97.4; bovine serum albumin, 66.0; glutamic dehydrogenase, 55.4; lactate dehydrogenase, 36.5; carbonic anhydrase, 31.0; trypsin inhibitor, 21.5; lysozyme, 14.4; aprotinin, 6.0.

microsequencing. We have determined the identities of each of the smaller polypeptides by amino-terminal sequencing, since the predicted M_r for T4MOB and T4MOD are similar (9.6 and 11.6 kDa, respectively) and because these two polypeptides co-elute from several chromatographic steps (see below). For the more intensely staining smaller protein, this determination yielded the sequence XXFPVHAAFEKD-FLV. Except for the residues from the first two cycles, which could not be unambiguously identified,[2] the determined sequence exactly matched that predicted from translation of the *tmoB* gene sequence. The less intensely staining polypeptide was confirmed to be T4MOD, since the determined sequence XTLADQALHNNNVGPII[2] exactly matched that predicted from translation of the *tmoD* gene sequence. Upon the basis of examination of numerous denaturing gels, the T4MOD protein appears to be present in a substoichiometric amount relative to the T4MOB in all of our T4MOH preparations. However, the T4MOD protein could also be purified in substantial quantities in an unbound form (Figure 3, lane 3), and, as described below, the addition of the separately purified T4MOD had a mildly stimulatory effect on the rate of the multiple-turnover hydroxylation reaction. These observations suggest that the T4MOH is a multisubunit protein consisting of the T4MOA, T4MOB, and T4MOE polypeptides, having a minimal native $M_r \approx 106$ kDa, and that the T4MOD can form a high affinity complex with the diferric form of T4MOH. Calibrated gel filtration measurements indicated that the T4MOH complex has $M_r \approx 220 \pm 20$ kDa, suggesting that the most plausible quaternary structure for the T4MOH is $(\alpha\beta\epsilon)_2$, with a variable amount of T4MOD bound after completion of the purification.

Physical and Spectroscopic Properties of T4MOH. The physical and spectroscopic properties of the T4MOH are summarized in Table 2. For comparative purposes, Table 2 also includes data obtained for the MMO hydroxylase and the stearoyl-ACP Δ^9 desaturase. The electronic absorption spectrum of the as-isolated T4MOH is featureless above 300 nm, indicating the absence of flavin, pterin, heme, iron−sulfur, or oxo-bridged diiron cofactors. Metal determinations revealed that the T4MOH contains variable amounts of iron (2−4 mol of Fe per mol of protein): no other metals were present. For other multicomponent aromatic oxygenases, such as TDO (Figure 1A), the addition of exogenous Fe^{2+} stimulated the oxygenase activity (Batie et al., 1987; Ensley & Gibson, 1983).[3] In contrast, the addition of exogenous Fe^{2+}, Fe^{3+}, Cu^{2+}, Mn^{2+}, or Zn^{2+} (50 μM) to assays of the T4MOH (10 μM) had no stimulatory effect on the catalytic turnover. As determined by quantitative EPR spectroscopy, a $g = 4.3$ signal observed from the as-isolated T4MOH always accounted for less than 0.1 spin per mol, indicating that the active site does not contain a high-spin ferric center. The chemical nature of the majority of the iron in the T4MOH was therefore most efficiently determined through the use of Mössbauer spectroscopy.

Figure 4B shows a 4.2 K Mössbauer spectrum of as-isolated (oxidized) T4MOH. This spectrum was best fit by two overlapping quadrupole doublets with parameters $\delta(1) = 0.51$ mm/s, $\Delta E_Q(1) = 0.93$ mm/s (85% of total Fe) and $\delta(2) = 0.56$ mm/s, $\Delta E_Q(2) = 1.55$ mm/s (15% of total Fe, contribution shown as the *solid* line above the data in Figure 4B).[4] These parameters are consistent with the presence of high-spin ferric ions and are typical of those reported for other diiron enzymes (see Table 2). Figure 4C shows the 4.2 K spectrum of the T4MOH recorded in an applied magnetic field of 8.0 T. We have analyzed this spectrum with the assumption that all iron atoms in the sample reside in diamagnetic ($S = 0$) environments. The close match of the spectral simulation with the data confirms the assumption of diamagnetism and suggests that the ferric sites belong to antiferromagnetically coupled ($H_{ex} = J\mathbf{S}_1\cdot\mathbf{S}_2$, $J > 0$) diiron centers. As discussed for the diferric MMO hydroxylase (Fox et al., 1993a), the first excited state of the spin-coupled center has $S = 1$ and is at energy J above the electronic ground state. By measuring the temperature dependence of the Mössbauer spectrum in strong applied magnetic fields, the magnitude of the exchange coupling can be assessed. Figure 4D shows the 8.0 T spectrum recorded at 23 K. Note that the absorption bands of the 23 K spectrum are slightly broader than those observed at 4.2 K. Moreover, the intensity of the central feature has increased at 23 K. These changes indicate population of the $S = 1$ multiplet. In evaluating the 23 K spectrum, three cases can be considered. If the electronic spin would undergo fast relaxation among the thermally populated levels, namely, the $S = 0$ and $S = 1$ states, a single spectrum with sharp features and decreased magnetic splittings would result. Alternatively, in the long relaxation limit, each populated electronic level would produce a distinct Mössbauer spectrum with intensities

[2] The first two amino acids calculated from the *tmoB* and *tmoD* gene sequences were Met-Ser, and Met-Thr, respectively. *N*-formyl-Met was not identified by the amino-terminal sequencing protocol used for the present studies. Likewise, an unambiguous identification of Ser or Thr can be problematic during amino-terminal sequencing.

[3] The aromatic ring dioxygenases that contain a Rieske iron−sulfur center in the oxygenase active site (e.g., TDO, Figure 1A) are activated by the *in vitro* addition of ferrous ion, which can apparently undergo reversible association and dissociation from a mononuclear iron catalytic site.

[4] The observation of two quadrupole doublets with intensity ratio 0.85/0.15 implies that our T4MOH sample contains two populations of molecules with different diiron centers. This phenomenon has been observed for MMO (Fox et al., 1993a; Liu et al., 1995a) and the stearoyl-ACP Δ^9 desaturase (Fox et al., 1993b). For the latter protein, we have recently eliminated the minority species by addition of the glassing agent isopropanol (J. Broadwater, B. G. Fox, C. Achim, and E. Münck, unpublished data).

Table 2: Comparison of Physical and Spectroscopic Properties of the Diiron Centers in *P. mendocina* KR1 T4MOH,[a] Methane Monooxygenase Hydroxylase,[b] and Stearoyl-ACP Δ^9 Desaturase[c]

parameter	T4MOH	methane monooxygenase	stearoyl-ACP desaturase
MW (kDa)	220 ± 20	254	84
subunit structure	$(\alpha\beta\gamma)_2$	$(\alpha\beta\gamma)_2$	α_2
iron content	3 ± 1	4	4
diferric state			
absorption maxima[d] (nm)	280	280	280, 325, 358, 470, 600
E_Q, δ (mm/s)[e]	0.93, 0.51 (85%)	1.16, 0.52	1.54, 0.53
	1.55, 0.56 (15%)	0.91, 0.51	
mixed valence state			
g values	not observed[f]	1.98, 1.94, 1.76	not observed[f]
E_Q, δ (mm/s) Fe^{2+}		1.19, 2.4	
ΔE_Q, δ (mm/s) Fe^{3+}		0.48, −1.3	
diferrous state			
g values[g]	≈16	≈16	not observed[f]
δ (mm/s)	1.31	1.3	1.30, 1.30
E_Q (mm/s)	3.21, 2.68	∼3.0, ∼2.7	3.36, 3.04

[a] Present work. [b] Data for Me_2SO complexes from Fox et al. (1993a). [c] Data from Fox et al. (1993b). [d] Stearoyl-ACP desaturase contains a μ-oxo-bridged diiron center, giving rise to $O^{2-} \rightarrow Fe^{3+}$ charge transfer bands in the visible region. The methane monooxygenase has a hydroxo-bridged diiron center, which has no detectable charge transfer features: a similar assignment is consistent for the T4MOH. [e] 4.2 K Mössbauer parameters for two inequivalent diiron center sites in T4MOH and MMOH. Isomer shifts are measured relative to Fe metal at 298 K. [f] The mixed valence state has not been observed for T4MOH or stearoyl-ACP desaturase. Moreover, the stearoyl-ACP desaturase does not exhibit an integer-spin EPR at X-band. [g] The observed resonances for the integer-spin EPR signal arise from the diferrous center; effective g values are quoted.

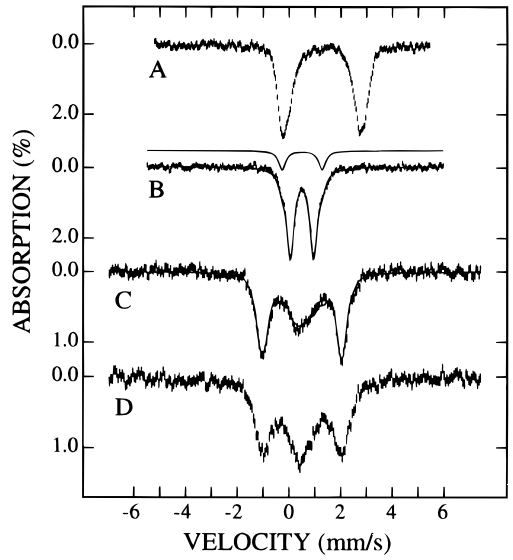

FIGURE 4: Mössbauer spectra of the ^{57}Fe-enriched T4MOH. (A) 4.2 K zero-field spectrum of reduced T4MOH. (B) 4.2 K zero-field spectrum of the as-isolated (i.e., oxidized) T4MOH. The solid line is a least-squares fit assuming two doublets with $\Delta E_Q(1) = 0.89$ mm/s and $\delta(1) = 0.51$ mm/s (85% of total Fe) and $\Delta E_Q(2) = 1.55$ mm/s and $\delta(2) = 0.56$ mm/s (15% of total Fe). The doublet of minority species 2 is shown separately above the data. (C) 4.2 K spectrum of as-isolated T4MOH recorded in an 8.0 T field applied parallel to the observed γ-radiation. The solid line is a spectral simulation assuming that all iron sites reside in diamagnetic environments. (D) 8.0 T spectrum of as isolated T4MOH recorded at 23 K. Protein data: 1.2 mM T4MOH protein; 3 ± 1 mol of iron per mol of T4MOH.

governed by Boltzmann factors. By examination of computer-generated simulations, we could readily verify that neither situation applies for T4MOH. Rather, the relaxation of the electronic spin is intermediate, and the data can only be analyzed by adopting a relaxation model that is beyond the scope of the present paper. However, even without a detailed analysis, it is apparent that the $S = 1$ multiplet is appreciably populated at 23 K, suggesting a J value in the range 15 cm^{-1} $< J <$ 30 cm^{-1}. Synthetic diiron model complexes containing hydroxo or alkoxo bridges have J values of 15−35 cm^{-1} (Kurtz, 1990), while a J value of 180−240 cm^{-1} is characteristic of an oxo-bridged diiron center (Kurtz, 1990). For example, ribonucleotide reductase contains an oxo-bridged diiron center and has $J = 216$ cm^{-1} (Petersson et al., 1980). Oxo-bridged diiron centers also exhibit characteristic ligand to metal charge transfer interactions in the visible region around 350 nm, while hydroxo-bridged diiron centers exhibit no such interactions (Kurtz, 1990). Using this information, and by comparison with the optical and Mössbauer data obtained for MMO (Fox et al., 1993a), we conclude that the majority species of T4MOH has a diiron center that does not contain an oxo bridge, but instead contains hydroxo or perhaps alkoxo bridges (Fox et al., 1993a; Rosenzweig et al., 1995) in the diferric state.

Upon partial reduction, several of the known diiron proteins (MMO, rubrerythrin, purple acid phosphatase, hemerythrin) exhibit an EPR signal characteristic of a mixed valence diiron center [$S = {}^1/_2$, $g_{ave} = 1.85$, all g values below $g = 2$; see Que and True (1990) for a review]. Addition of substoichiometric quantities of sodium dithionite to anaerobic preparations of the T4MOH failed to produce samples exhibiting an EPR signal characteristic of the mixed valence state. However, the addition of sodium dithionite in the presence of the redox mediator methyl viologen directly converted the diiron center to the *diferrous* state. The 4.2 K Mössbauer spectrum of the reduced T4MOH, shown in Figure 4A, exhibits a quadrupole doublet with features typical of high-spin ($S = 2$) Fe^{2+}, demonstrating that all of the iron in the T4MOH can be reduced by the anaerobic addition of sodium dithionite. The features of this doublet can be adequately represented as a superposition of two unresolved doublets, with parameters $\delta(1) = \delta(2) = 1.31$ mm/s, and $\Delta E_Q(1) = 3.21$ mm/s, $\Delta E_Q(2) = 2.68$ mm/s. This decomposition, which is not unique, nevertheless suggests two inequivalent sites. The isomer shifts observed for both ferrous sites further suggest an octahedral coordination environment that is rich in oxygen ligands (such as carboxylate or water). In general, the two ferrous sites of reduced diiron proteins are coupled by exchange interactions ($H_{ex} = J\mathbf{S}_1 \cdot \mathbf{S}_2$). For strong antiferromagnetic coupling ($J >$ 0), the ground state of the dinuclear system will be

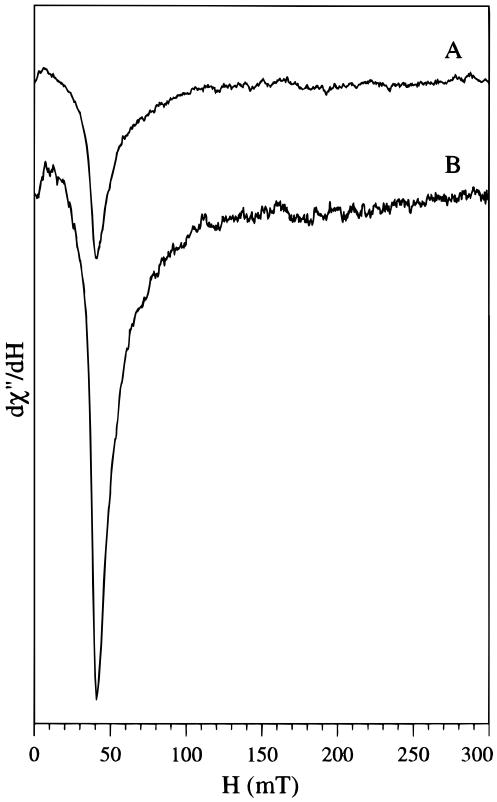

FIGURE 5: X-band EPR spectra of the reduced T4MOH recorded with a bimodal cavity in parallel mode. (A) 11 K. (B) 5 K. Instrumental conditions: 10 mW; 9.34 GHz; 10 G modulation amplitude; 100 kHz modulation frequency; scan range 0−300 mT; scan time 8 min. The spectrum was obtained on an aliquot of the Mössbauer sample from Figure 4A.

diamagnetic. In contrast, for ferromagnetic coupling ($J < 0$), the coupled ground state will be paramagnetic. Figure 5 shows low temperature EPR spectra of reduced T4MOH, obtained at 11 and 5 K. The broad feature centered around $g \approx 16$ is similar to that observed for reduced MMO and is characteristic for a system with integer electronic spin (Hendrich et al., 1990; Münck et al., 1993). While the observation of a $g \approx 16$ resonance rules out *strong* antiferromagnetic coupling, this resonance is compatible with either strong ferromagnetic coupling or weak (either ferromagnetic or antiferromagnetic) coupling (the terms *strong* and *weak* refer to the strength of the exchange coupling relative to the zero-field splitting of the ferrous sites of diiron proteins, typically, $|D| \approx 5$ cm^{-1}).

Physical and Spectroscopic Properties of T4MOC. Figure 3, lane 4, shows a denaturing polyacryamide gel analysis of the purified T4MOC. The T4MOC was first identified by comparison with the work of Whited and Gibson (1991), who purified the T4MOC to homogeneity using chromatographic conditions nearly identical to those described here. The anomalous migration of T4MOC in denaturing gels has been previously noted (Yen et al., 1991; Whited & Gibson, 1991). However, in the electrophoresis buffer system used in the present study (Schägger & von Jagow, 1987), the T4MOC has $M_r \approx 14$ kDa, consistent with that predicted from translation of the gene sequence (12 326 Da). Moreover, on the basis of calibrated gel filtration measurements, the T4MOC appears to be a monomeric protein.

The identity and function of the T4MOC have now been unambigously determined based upon the spectroscopic and

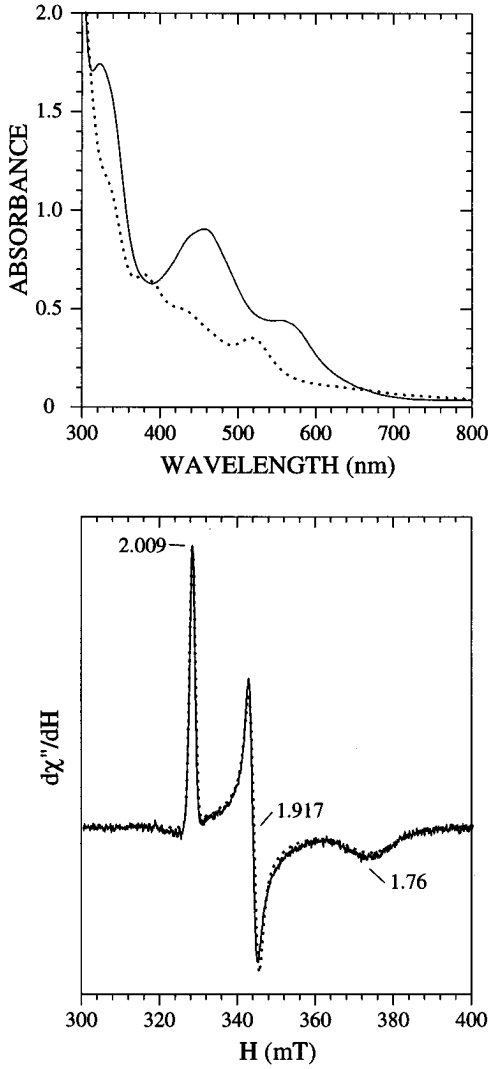

FIGURE 6: Optical and X-band EPR spectra of T4MOC. (A) (Solid line) Optical spectrum of the as-isolated T4MOC and (dotted line) spectrum of the reduced T4MOC. (B) X-band EPR spectrum of the reduced TMOC recorded at 10 K. The solid line is a spectral simulation for a spin $S = {}^1/_2$ system with $g_x = 1.917$, $g_y = 1.76$, and $g_z = 2.009$. In order to account for the width of the lines, we have assumed that the principal g values are distributed about their mean values with Gaussian widths $\sigma_x = 0.006$, $\sigma_y = 0.027$, and $\sigma_z = 0.004$. Instrumental conditions: 10 K; 0.1 mW; 9.46 GHz; 10 G modulation amplitude; 100 kHz modulation frequency; scan range 300−450 mT; scan time 8 min. Protein data for the EPR sample: 0.6 mM TMOC protein; 2.03 ± 0.06 mol of Fe per mol of TMOC; spin quantitation relative to a 1 mM $CuSO_4$ standard gave 0.95 spin per mol of TMOC.

catalytic properties described in Figures 6−8 and Tables 3−5. The T4MOC contains 2.03 ± 0.06 mol of iron per mol protein; no other metals were detected by EPR or plasma emission spectroscopy. The T4MOC exhibits electronic absorption bands (see Table 3 and Figure 6, top panel, solid line) whose absorption maxima differ significantly from the spectra of [2Fe-2S] centers coordinated to four cysteinyl residues such as putidaredoxin and other plant-type [2Fe-2S] ferredoxins but are quite similar to ferredoxins with mixed Cys and His ligation, namely, the Rieske-type iron−sulfur center (Fee et al., 1984; Gurbiel et al., 1989; Cline et al., 1985). Due to the requirement of T4MOC for multiple-turnover catalysis (see below), we have used Mössbauer and EPR spectroscopies to define the physical properties of the T4MOC iron center.

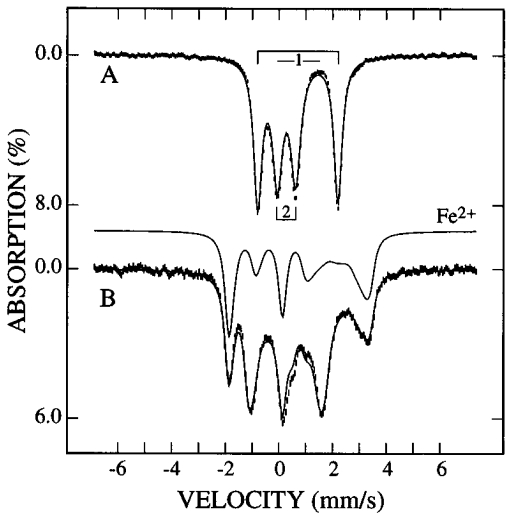

FIGURE 7: 200 K Mössbauer spectra of reduced TMOC. The spectra were obtained from a more highly concentrated preparation than that used to obtain the spectra of Figure 8. (A) Spectrum recorded in zero field. The solid line is the result of least-squares fitting two doublets of equal intensity to the data. (B) Spectrum recorded in an 8.0 T magnetic field applied parallel to the observed γ-radiation. The solid lines are spectral simulations generated from eq 1 using the parameters listed in Table 3. The spectral contribution of the ferrous site is drawn separately above the data of spectrum B.

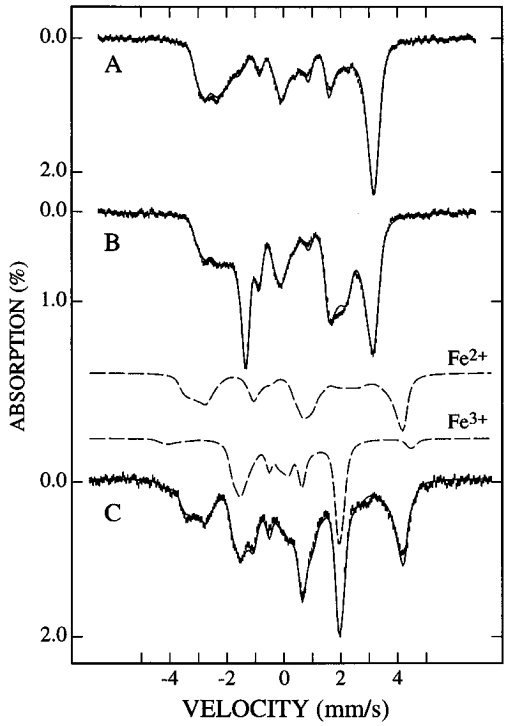

FIGURE 8: 4.2 K Mössbauer spectra of the reduced TMOC. Spectra were recorded in parallel fields of 45 mT (A) and 6.0 T (C) and in a transverse field of 45 mT (B). The solid lines are spectral simulations generated from eq 1 using the parameters listed in Table 3. The dashed lines shown above the data of spectrum C are spectral contributions of the individual iron sites.

The Mössbauer spectrum of oxidized T4MOC (not shown) recorded at 4.2 K in zero applied field consists of two nested quadrupole doublets with narrow ($\Gamma = 0.26$ mm/s) absorption lines of Lorentzian shape that account for all iron in the protein sample. From least-squares fitting, we obtained $\delta(1) = 0.35$ mm/s, $\Delta E_Q(1) = 1.12$ mm/s, and $\delta(2) = 0.24$ mm/s, $\Delta E_Q(2) = 0.51$ mm/s. These parameters are very similar to those reported for the Rieske iron−sulfur protein from *Thermus thermophilus* (Fee et al., 1984). The absence of magnetic hyperfine interactions in the 4.2 K spectrum is consistent with the presence of an antiferromagnetically coupled pair of high-spin ferric ions, while isomer shifts between 0.20 and 0.30 mm/s are characteristic of Fe^{3+} sites in a tetrahedral environment of thiolate and sulfide ligands. The distinctly larger isomer shift observed for site 1 suggests a mixed sulfide/histidine coordination that is also characteristic of the Rieske-type iron center.

Figure 6 (top panel, dotted line) shows the optical spectrum of the reduced T4MOC. The intensities of the absorbance bands at 328 and 456 nm decrease by ~50% upon reduction, while two new absorption bands appear at 380 and 520 nm. Figure 6 (bottom panel, solid line) shows the corresponding 10 K EPR spectrum of the reduced T4MOC. The observed g values, $g_x = 1.917$, $g_y = 1.76$, and $g_z = 2.009$, and the corresponding line widths are typical for Rieske-type proteins (Bertrand & Gayda, 1979). The dotted line drawn through the EPR data is a spectral simulation for a spin $S = {}^1/_2$ system using the above quoted g values. In order to account for the widths of the lines, we have assumed that the principal g values are distributed about their mean values with Gaussian widths $\sigma_x = 0.006$, $\sigma_y = 0.027$, and $\sigma_z = 0.004$.

Figures 7 and 8 show Mössbauer spectra of the reduced T4MOC. The 200 K spectrum of Figure 7A, recorded under conditions where the electronic spin $S = {}^1/_2$ of the $[2Fe\text{-}2S]^{1+}$ center relaxes fast on the time scale of Mössbauer spectroscopy, exhibits two nested doublets. The innermost doublet has $\Delta E_Q(2) = 0.68$ mm/s and $\delta(2) = 0.25$ mm/s at 200 K; because of a temperature-dependent second-order Doppler shift, $\delta(2) \cong 0.30$ mm/s at 4.2 K. Thus, doublet 2 reflects a ferric site, most probably the site 2 quoted for the oxidized protein. The outer doublet of the reduced protein has $\Delta E_Q(1) = 3.07$ mm/s and $\delta(1)$ is 0.70 mm/s at 4.2 K. As pointed out previously (Fee et al., 1984), site 1 clearly reflects a ferrous site.

The 4.2 K spectra of Figure 8 display intricate magnetic patterns that are characteristic for the Rieske-type iron−sulfur center. Since the spectra of T4MOC are very similar to those reported for the *T. thermophilus* Rieske protein, the data analysis for T4MOC can be carried out as previously reported (Fee et al., 1984). Thus, we have fitted the Mössbauer spectra of Figures 7 and 8 to the $S = {}^1/_2$ spin Hamiltonian

$$\boldsymbol{H} = \beta \mathbf{S}\cdot g\cdot \mathbf{H} + \sum_{i=1}^{2}\left\{ \mathbf{S}\cdot\mathbf{A}(i)\cdot\mathbf{I}(i) - g_n\beta_n\mathbf{H}\cdot\mathbf{I}(i) + \frac{eQV_{zz}(i)}{12}\left[3\mathbf{I}_z^{\,2}(i) - \frac{15}{4} + \eta(i)(\mathbf{I}_x^{\,2}(i) - \mathbf{I}_y^{\,2}(i))\right]\right\} \quad (1)$$

where $i = 1, 2$ sums over the ferrous and ferric sites, respectively, and where all symbols have their conventional meanings. The solid lines drawn through the spectra of Figures 7 and 8 are simulations based on eq 1 using the parameters listed in Table 3. The dashed lines above the 6.0 T spectrum of Figure 8C give the contributions of the ferrous and ferric sites separately. It can be seen from inspection of the low temperature spectra that the magnetic splitting of the ferrous site increases with increasing applied field, while that of the ferric site decreases. As pointed out elsewhere (Münck et al., 1972; Sands & Dunham, 1975), this behavior determines the signs of the magnetic hyperfine

Table 3: Optical Data, *g* Values, and Hyperfine Parameters of *P. mendocina* KR1 T4MOC and *T. thermophilus* Rieske Proteins

parameter	T4MOC[a]		T. thermophilus[b]	
oxidized state				
absorption maxima (nm)	280, 325, 458, 560		325, 458, 560	
δ (mm/s)[c]	0.35(1),[d] 0.24(1)		0.32, 0.24	
E_Q (mm/s)[c]	1.12(1), 0.52(1)		0.91, 0.52	
reduced state ($S = {}^1/_2$)				
g values	1.917, 1.760, 2.009		1.90, 1.80, 2.02	
	ferric site	ferrous site	ferric site	ferrous site
δ (mm/s)	0.30(1)	0.72(2)	0.31	0.74
E_Q (mm/s)	0.71(2)	−3.07(3)	0.63	−3.05
η	0	3[e,f]	0	3[e]
A_x (MHz)	−56(1)	15.5(1)	−55	14
A_y (MHz)	−48(1)	12(1)	−50	11
A_z (MHz)	−42(1)	33(1)	−43	33

[a] Present work. [b] Data from Fee et al. (1984). [c] Mössbauer parameters for two inequivalent iron sites at 4.2 K. [d] Numbers in parentheses are estimated uncertainties in least significant digits. [e] A value of $\eta = 3$ describes an electric field gradient with axial symmetry around the *y*-axis. When quoted in the principal axis system of the electric field gradient tensor (ξ,η,ζ) and using the convention $|V_{\xi\xi}| \geq |V_{\eta\eta}| \geq |V_{\zeta\zeta}|$ with $\eta = (V_{\zeta\zeta} - V_{\eta\eta})/V_{\xi\xi}$, the values $\Delta E_Q = -3.07$ mm/s and $\eta = 3$ become $\Delta E_Q = +3.07$ mm/s and $\eta = 0$. [f] In the (ξ,η,ζ) frame, the uncertainty is $0 \leq \eta \leq 0.3$.

Table 4: Protein Components of Toluene-4-monooxygenase Required for the Single-Turnover Formation of *p*-Cresol

components added	*p*-cresol formation (nmol)
reduced T4MOC alone (100)	0
T4MOD alone (100)	0
reduced T4MOH alone (100)	8
+ reduced T4MOC (200)	17
+ oxidized T4MOC (200)	8
+ T4MOD (200)	8
+ oxidized T4MOC (200), T4MOD (200)	8

[a] Single-turnover reactions performed using 100 nmol samples of the T4MO components prepared as described in Materials and Methods. The nanomolar amounts of the components added to the single-turnover reactions are indicated in parentheses.

Table 5: Multiple-Turnover Reconstitution of the Toluene-4-monooxygenase Complex

components added	*p*-cresol formation (milliunits/mg)
control reaction[b,c]	285
minus T4MOH	0
minus T4MOF	0
minus T4MOC	<3
minus T4MOD	196
plus 0.6 nmol T4MOD	281
plus 1.3 nmol T4MOD[b,c]	285
plus 2.5 nmol T4MOD	226
plus 5.0 nmol T4MOD	224
plus 25.0 nmol T4MOD	152

[a] Specific activity of the T4MOH present in the assay. [b] The control reaction contained 2.5 nmol of T4MOH, 2.5 nmol of T4MOC, 1.3 nmol of T4MOD, ~2.5 nmol of T4MOF, 0.25 μmol of NADH, and 5 μmol of toluene in 250 μL of 50 mM phosphate buffer, pH 7.5, at 25 °C. [c] The specific activities for the other individual components (milliunits/mg) were as follows: T4MOC, 18 000; T4MOD, 19 400. [c] The total amount of T4MOD was increased as indicated.

tensors, **A**, and establishes that the system spin $S = {}^1/_2$ of the ground state results from antiferromagnetic coupling between ferrous ($S_2 = 2$) and ferric ($S_1 = {}^5/_2$) sites.

In a previous study of the $[2Fe\text{-}2S]^{1+}$ center of the MMO reductase component, we have pointed out that the *A* values of the ferrous site are strongly correlated with the asymmetry parameter, η, of the electric field gradient tensor. Thus, a family of *A* and η values yields virtually identical fits to the Mössbauer spectra [see Figure 18 of Fox et al. (1993a)]. However, under favorable circumstances, η can be reasonably well determined when the spectra are studied in strong applied fields at high temperature; in a proper coordinate frame, the range of η is constrained to $0 \leq \eta \leq 1$. In order to achieve good signal/noise at 200 K, we prepared a sample ~3-fold more concentrated than the one used to record the spectra of Figure 8 and recorded the 8.0 T spectrum. The spectral simulation shown in Figure 7B was determined from this spectrum and establishes that $\eta \leq 0.3$, thus constraining the *A* values of the ferrous site in the T4MOC Reiske center as indicated in Table 3.

Single-Turnover Activity. The physical properties reported above are consistent with the T4MOH having a hydroxylase function and the T4MOC having an electron transfer function in the T4MO complex. However, since a Rieske-type [2Fe-2S] center is found in the active site of the *cis*-dihydrodiol-forming aromatic dioxygenases (Mason & Cammack, 1992), and since the reduced T4MOC was found to be reversibly and quantitatively reoxidized in the presence of air ($t_{1/2} \approx$ 0.5 min), we have investigated the possibility that the T4MO active site could be uniquely assembled from a complex of T4MOC and T4MOH components by using single-turnover catalytic studies. Table 4 shows that, under single-turnover conditions, the T4MOH alone could catalyze the oxidation of toluene to *p*-cresol, while the combination of the T4MOH and the reduced form of T4MOC provided a slightly higher yield in the single-turnover reaction than from the T4MOH alone. Neither the T4MOC nor T4MOD alone were capable of the single-turnover hydroxylation of toluene, while the further addition of the T4MOD (~2-fold molar excess) to either the T4MOH or the T4MOH and T4MOC did not appreciably change the yield of the single-turnover reaction obtained from T4MOH alone. Thus, the single-turnover experiments summarized in Table 4 provide evidence that the T4MOH alone functions as the oxygenase component of the T4MO complex. These experiments are also consistent with the function of the T4MOC as an electron transfer protein, since the presence of the reduced T4MOC increased the single-turnover yield, presumably by promoting additional electron transfer events.

Multiple-Turnover Reconstitution of T4MO Activity. The results of multiple-turnover experiments using NADH as the source of reducing equivalents are summarized in Table 5. For the reconstituted enzyme complex, no *p*-cresol formation

was detected after the single omission of either the T4MOH or the T4MOF, and very low activity was observed after omission of the T4MOC. The absolute requirement for T4MOH is consistent with the hydroxylase function assigned on the basis of the single-turnover reactions. In the presence of the T4MOC, the rate of the NADH-dependent hydroxylation reaction catalyzed by T4MOH and T4MOF was increased by more than 100-fold, which also supports an essential functional role for T4MOC in mediating electron transfer between T4MOF and T4MOH. Moreover, the specificity of electron transfer from T4MOC to the T4MOH appears to be a direct consequence of protein structure: neither spinach ferredoxin nor the vegetative ferredoxin from *Anabena* PCC 7120 could substitute during multiple-turnover oxidation of toluene. In contrast, our partially purified fractions of T4MOF could be substituted by the use of spinach ferredoxin reductase and NAD(P)H as the oxidoreductase component (Zanetti & Curti, 1980), in combination with the T4MOC.

During the first two steps of the purification of the T4MOH, a substantial fraction of the total T4MOD produced by the expression system copurifies with the fractions containing hydroxylase activity. For these fractions, the further addition of purified T4MOD to reaction assays did not stimulate the hydroxylation rate of the reconstituted enzyme complex. However, after the third step of the purification of the T4MOH has been completed, the further addition of T4MOD could provide a modest stimulation of the hydroxylation rate (Table 5), suggesting that the amount of T4MOD in the purified complex had been depleted. Optical, EPR, and plasma emission measurements have revealed that the purified T4MOD contains no metal ions or organic cofactors, suggesting that protein−protein interactions form the basis of this catalytic stimulation. Since the T4MOD has limited amino acid sequence homology with the MMO component B (Johnson & Olsen, 1995), we have presently assigned the T4MOD to function as an effector of the T4MO catalytic activity.

DISCUSSION

The existence of several structurally distinct enzyme complexes catalyzing monooxygenation reactions at all possible positions on the toluene molecule represents a fascinating example of evolutionary adaptation. This variation in regiospecificity is provided by a membrane-bound enzyme (xylene monooxygenase, Figure 1B) as well as three additional soluble enzyme complexes (T2MO, T3MO, and T4MO, Figure 1C−E respectively). The present work has shown that the T4MO from *P. mendocina* KR1 is a multicomponent monooxygenase complex with a previously unrecognized composite structure. The hydroxylase component (T4MOH) is a dimeric protein composed of three subunits [polypeptides T4MOA, T4MOB, and T4MOE, $(\alpha\beta\epsilon)_2 \approx 220$ kDa] that contains catalytically competent diiron centers. The T4MOD (11.6 kDa) can be copurified as a substoichiometric constituent of the T4MOH; in addition, the T4MOD can be purified as a separate soluble protein that has mildly stimulatory effect on the steady-state turnover of the purified complex. The properties of these two purified T4MO components appear to be closely related to the hydroxylase and component B of the soluble MMO complex (Lipscomb, 1994) and the T2MO hydroxylase and small protein recently isolated from *Burkholderia cepacia* G4 (Newman & Wackett, 1995). These latter two complexes also use a single iron−sulfur flavoprotein oxidoreductase to mediate electron transfer between NADH and the diiron hydroxylase. In contrast, the T4MO electron transfer chain consists of both an NADH oxidoreductase (T4MOF, 36 kDa) and a Rieske-type ferredoxin (T4MOC, 12.5 kDa). The T4MOC is obligately required for efficient electron transfer between T4MOF and T4MOH, and optimal levels of T4MOC provide a dramatic increase in the hydroxylation rate. The requirement for *two* electron transfer proteins is structurally most closely related to the electron transfer chains of the *cis*-dihydrodiol forming aromatic dioxygenases, such as TDO from *P. putida* F1 (Wackett, 1990) and the napthalene dioxygenase complex from *Pseudomonas* sp. Strain 9816-4 (Gibson et al., 1995)

Purification of the T4MO Complex. The pRS202 expression system provides cell-free extracts with sufficient catalytic activity that *p*-cresol formation can be reliably assayed using gas chromatography as a substitute for the previously used radiometric methods (Yen et al., 1991; Whited & Gibson, 1991; Newman & Wackett, 1995). Anion exchange chromatography separates the cell-free extract into three fractions that can be reconstituted into a catalytically active enzyme complex: one fraction contains both T4MOD and T4MOF; a second contains a T4MOH and T4MOD complex; and the third contains T4MOC. The first ion exchange step described here is comparable to that previously developed for the fractionation of *P. mendocina* KR1 cell-free extracts, where three fractions, called A, B, and C, were obtained (Whited & Gibson, 1991). It is likely that fraction A obtained from *P. mendocina* KR1 contained a mixture of both T4MOD and T4MOF, while fractions B and C were correctly identified as the hydroxylase and ferredoxin components, respectively. In these previous efforts, further purification of fraction A resulted in the loss of reconstitutable enzyme activity, possibly due to inactivation of T4MOF. We have observed that only a small amount of T4MOF is produced in the recombinant host, and that the activity of the partially purified T4MOF can be enhanced by the addition of FAD, suggesting the loss of a cofactor may potentially contribute to the lability of this component. Due to loss of activity at later steps in the purification, we have not yet developed a complete purification or obtained a detailed physical characterization of this component. Nevertheless, the partially purified T4MOF exhibits absorption maxima at ∼340, 400, and 470 nm and a shoulder between 525 and 600 nm. Although not conclusive, these features are consistent with the proposed presence of both flavin and [2Fe-2S] domains in the T4MOF based on amino acid sequence analysis (Yen & Karl, 1992).

Structural and Catalytic Properties of the T4MOH Component. Tables 1 and 5 show that the T4MO complex has a reconstituted specific activity for the oxidation of toluene of ∼250−350 milliunits/mg, stated with respect to the T4MOH component. The specific activities of the T4MOC and the partially purified T4MOF components in the toluene hydroxylation reaction are also indicated in these tables.

The T4MOA polypeptide contains two copies of the amino acid sequence motif $(D/E)X_{(28-32)}DEXRH$ (Yen et al., 1991), which provides the six protein-derived ligands to the spectroscopically and crystallographically characterized diiron centers in the MMO hydroxylase (Lipscomb, 1994; Rosenzweig et al., 1995). The presence of this motif

originally prompted our assignment of T4MO to the hydrocarbon hydroxylase subclass of the class II diiron proteins (Fox et al., 1994). This assignment has now been validated by Mössbauer, EPR, and optical studies of the diferric and diferrous redox states of the T4MOH. These measurements, in particular the lack of absorption in the visible region and the weak exchange coupling (*J)* in the diferric state, suggest that the T4MOH diiron center will contain hydroxo bridge(s), as has been reported for the diferric center of MMO (Rosenzweig et al., 1993; Fox et al., 1994). Thus, the disposition of oxygen atom bridge(s) in the diferric centers of the presently purified diiron hydroxylases (MMO hydroxylase, T4MOH, and T2MOH) consistently differs from the oxo-bridged diiron centers found in the R2 component of ribonucleotide reductase (Sjöberg et al., 1982) and stearoyl-ACP Δ^9 desaturase (Fox et al., 1994). Although the mechanistic implications of this structural variation remain to be fully defined, the presence of potentially dissociable protons within the active site of the hydroxylases may indeed be associated with the course and outcome of the oxygen activation chemistry. The presence of an integer-spin EPR signal in the diferrous state and the single-turnover competence of the diferrous T4MOH alone also indicate that the T4MOH diiron center has properties most similar to the diiron center contained in the MMO hydroxylase (see Table 2).

Nucleotide sequences for the toluene ortho-, meta-, and para-hydroxylation complexes have been published (Yen et al., 1991; Byrne et al., 1995; Johnson & Olsen, 1995). In addition, nucleotide sequences of a structurally related multicomponent phenol hydroxylase (Nordlund et al., 1990), an alkene monooxygenase (Saeki & Furuhashi, 1994), and the soluble MMO from two different methanotrophic species have been reported (Stainthorpe et al., 1990; Cardy et al., 1991). Comparisons of percent identity, percent similarity (Johnson & Olsen, 1995), and evolutionary distances strongly suggest that this entire group of bacterial hydrocarbon oxidation enzymes comprises an evolutionarily related protein family. Most importantly, all of the polypeptides containing the diiron center motif retain key residues associated with the iron ligands, hydrogen bonding networks (Fox et al., 1994; Rosenzweig et al., 1993), and putative surface of the active site pocket (Rosenzweig et al., 1995). However, other residues within the proposed active site pocket differ, providing a yet-to-be elucidated example of how natural variations in protein structure may lead to diversity of catalytic outcome.

Recently, the hydroxylase component of T2MO has been reported to function as a catalase in the presence of exogenous H_2O_2, with the catalase reaction rate exceeding the hydroxylation reaction rate by 100 000-fold (Newman & Wackett, 1995). The ability to perform the catalase reaction would represent a mechanistically important variation on the known versatility of the known diiron enzymes, and we were thus interested to determine if T4MOH could also catalyze this type of reaction. A significant level of catalase activity was detected in cell-free extracts containing the T4MO complex, as is commonly observed in cell extracts prepared from many species of aerobic bacteria. However, during each step of the purification of the T4MOH, the fractions containing the maximal catalase activity *did not* correspond to the fractions containing the maximal toluene hydroxylation activity. We have found that *E. coli* catalase behaves similarly to T4MOH during both anion exchange (elution at ~0.25 and 0.35 M NaCl, respectively, at pH 7.0), and gel filtration (~250 versus ~220 kDa, respectively) chromatographies. In addition, bacterial catalases generally exhibit high turnover numbers, up to 8×10^5 s^{-1}. Given these properties, a less than 0.1% (w/w) contamination could yield a catalase activity similar to that reported for the T2MO complex. In contrast, the T4MOH samples described here exhibit no detectable catalase activity yet retain full toluene hydroxylation activity. This absence of catalase activity in T4MOH is furthermore in accord with the results previously obtained for the MMO hydroxylase (Green & Dalton, 1985; Froland et al., 1992; Andersson et al., 1991).

The Mössbauer spectra of Figure 4B,C demonstrate the absence of mononuclear iron in the purified T4MOH. While the iron content of the purified T4MOH is somewhat lower than would be expected from the dimeric structure (4 mol of iron contained in two diiron centers), a variable content of iron has been a recurring problem in the enzymology of the diiron enzymes. For another recombinant diiron enzyme, the stearoyl-ACP Δ^9 desaturase, we have recently found that the level of iron incorporation is strongly influenced by the growth conditions used for the overexpression (Hoffman et al., 1995). Moreover, the nonspecific turnover of the recombinant T4MO system in the absence of suitable substrates may also contribute to the loss of iron from the enzyme due to oxidative damage (Green & Dalton, 1989).

Structural and Catalytic Properties of the T4MOC Component. An examination of amino acid sequences suggested that the T4MOC would contain a Rieske-type iron sulfur center (Yen et al., 1991), which has been confirmed by the EPR and Mössbauer studies reported here (see Table 3 and Figures 6−8). While ferredoxin proteins have been either purified (Powlowski & Shingler, 1990) or inferred from nucleotide sequences (Johnson & Olsen, 1995; Byrne et al., 1995) for all of the aromatic diiron hydroxylases, the function of these ferredoxins has not been clearly defined. We have found that the T4MOC is obligately required for reconstitution of NADH-dependent catalytic activity by mediating electron transfer between reductase proteins and T4MOH and can optimally yield a greater than 100-fold stimulation of multiple turnover activity. One possible explanation for the difference in the specific activities of the T4MOH (~300 milliunits/mg) and T2MOH (~2 milliunits/mg) is that a ferredoxin component could also be required in the latter enzyme complex. This explanation is supported by the presence of open reading frames having a Rieske-like motif *(tbuB)* in the T3MO operon from *Pseudomonas picketti* PKO1 (Byrne et al., 1995) and a ferredoxin-like motif *(tbmE)* in the T2MO operon from *Pseudomonas* sp. Strain JS150 (Johnson & Olsen, 1995).

Role of T4MOD in the T4MO Reaction. The presence of T4MOD in our purified samples of T4MOH suggested the possibility that the T4MOD protein may actually be a subunit of the T4MOH, as opposed to a separate protein component with high affinity for the diferric T4MOH. However, we have presently assigned the T4MOD to be a high-affinity component of the T4MO complex rather than a subunit of the T4MOH since the activity of T4MOH preparations partially depleted of T4MOD can be increased by the addition of separately purified T4MOD (see Table 5). This assignment is further supported by preliminary data obtained from study of an expression vector derived from pRS184f

that contains a deletion mutation spanning both the *tmoC* and *tmoD* genes. This vector produces a form of the T4MOH that exhibits catalytic activity only in the presence of exogeneously added T4MOC and T4MOD, thus supporting the ability of these proteins to freely associate into the correct complexes *in vitro*.

In light of the biochemical properties of the T4MOD reported here, a surprisingly conserved biochemical feature of the diiron hydroxylase complexes is the presence of this type of dissociable effector protein. By using the T4MOD protein as a query sequence, nine proteins having sequence similarity with the T4MOD can be identified: *tbuV* from the T2MO (Byrne et al., 1995), *tbmC* from the T3MO (Johnson & Olsen, 1995), orf3 (Z36909), phhM (X79063), phlC (X80765) and *dmpM* from the multicomponent phenol hydroxylase complexes (Nordlund et al., 1990), AMOB from alkene monooxygenase (Muira & Dalton, 1995), and the MMO component B proteins from *Methylococcus capsulatus* (Bath) (Stainthorpe et al., 1990) and *Methylosinus trichosporium* OB3b (Cardy et al., 1991). The MMO component B is presently the best characterized of these effector proteins and has previously been shown to increase the rate and yield of multiple turnover (Green & Dalton, 1985; Fox et al., 1991), perturb the spectral properties of the diiron center (Fox et al., 1991), change the product distribution obtained from the oxidation of complex substrates such as isopentane (Froland et al., 1992), and change the redox potential of the diiron center (Liu & Lippard, 1991; Paulsen et al., 1994). More recently, the component B has been shown to increase the rate of association of O_2 with the diferrous MMOH center, leading to the productive, sequential formation of the reactive intermediates compound P and compound Q prior to the oxidation of substrates (Liu et al., 1995b). The properties of the purified T4MOD reported here (complex formation with T4MOH, stimulation of steady-state turnover) suggest a related role in catalysis. However, since the affinity of the T4MOD for the diferric state of the T4MOH appears to be considerably higher than that recently determined for the interaction of the MMO hydroxylase and component B (Liu et al., 1995b), further efforts will be required to more fully define the function of the T4MOD. Nevertheless, it remains an interesting observation that the diiron center and the effector protein have been evolutionarily retained as separate components in all of the above-mentioned diiron hydroxylase complexes.

REFERENCES

Andersson, K. K., Froland, W. A., Lee, S.-K., & Lipscomb, J. D. (1991) *New. J. Chem. 15*, 411−415.

Batie, C. J., LaHaie, E., & Ballou, D. P. (1987) *J. Biol. Chem. 262*, 1510−1518.

Bertrand, P., & Gayda, J.-P. (1979) *Biochim. Biophys. Acta 579*, 107−121.

Byrne, A. M., Kukor, J. J., & Olsen, R. H. (1995) *Gene 154*, 65−70.

Cardy, D. L. N., Laidler, V., Salmond, G. P. C., & Murrell, J. C. (1991) *Mol. Microbiol. 5*, 335−342.

Cline, J. F., Hoffman, B. M., Mims, W. B., LaHaie, E., Ballou, D. P., & Fee, J. A. (1985) *J. Biol. Chem. 260*, 3251−3254.

De Lorenzo, V., Eltis, L., Kessler, B., & Timmis, K. N. (1993) *Gene 123*, 17−24.

Ensley, B. D., & Gibson, D. T. (1983) *J. Bacteriol. 155*, 505−511.

Fee, J. A., Findling, K. L., Yoshida, T., Hille, R., Tarr, G. E., Hearshen, D. O., Dunham, W. R., Day, E. P., Kent, T. A., & Münck, E. (1984) *J. Biol. Chem. 259*, 124−133.

Fischer, D. S., & Price, D. C. (1964) *Clin. Chem. 10*, 21−30.

Fox, B. G., Froland, W. A., Dege, J. E., & Lipscomb, J. D. (1989) *J. Biol. Chem. 264*, 10023−10033.

Fox, B. G., Froland, W. A., Jollie, D. R., & Lipscomb, J. D. (1990) *Methods Enzymol. 188*, 191−202.

Fox, B. G., Liu, Y., Dege, J. E., & Lipscomb, J. D. (1991) *J. Biol. Chem. 266*, 540−550.

Fox, B. G., Hendrich, M. P., Surerus, K. K., Andersson, K. K., Froland, W. A., Lipscomb, J. D., & Münck, E. (1993a) *J. Am. Chem. Soc. 115*, 3688−3701.

Fox, B. G., Shanklin, J., Somerville, C., & Münck, E. (1993b) *Proc. Natl. Acad. Sci. U.S.A. 90*, 2486−2490.

Fox, B. G., Shanklin, J., Ai, J., Loehr, T. M., & Sanders-Loehr, J. (1994) *Biochemistry 33*, 12776−12786.

Froland, W. A., Andersson, K. K., Lee, S.-K., Liu, Y., & Lipscomb, J. D. (1992) *J. Biol. Chem. 267*, 17588−17597.

Gibson, D. T., Hensley, M., Yoshioka, H., & Mabry, T. J. (1970) *Biochemistry 9*, 1626−1630.

Gibson, D. T., Resnick, S. M., Lee, K., Brand, J. M., Torok, D. S., Wackett, L. P., Schocken, M. J., & Haigler, B. E. (1995) *J. Bacteriol. 177*, 2615−2621.

Green, J., & Dalton, H. (1985) *J. Biol. Chem. 260*, 15795−15801.

Green, J., & Dalton, H. (1989) *J. Biol. Chem. 246*, 17698−17703.

Gurbiel, R. J., Batie, C. J., Sivaraja, M., True, A. E., Fee, J. A., Hoffman, B. M., & Ballou, D. P. (1989) *Biochemistry 28*, 4861.

Hendrich, M. P., Münck, E., Fox, B. G., & Lipscomb, J. D. (1990) *J. Am. Chem. Soc. 112*, 5861−5865.

Herrero, M., De Lorenzo, V., & Timmis, K. (1990) *J. Bacteriol. 172*, 6557−6567.

Hoffman, B. J., Broadwater, J. A., Johnson, P., Harper, J., Fox, B. G., & Kenealy, W. R. (1995) *Protein Express. Purif. 6*, 646−654.

Johnson, G. R., & Olsen, R. H. (1995) *App. Environ. Microbiol. 61*, 3336−3346.

Kurtz, D. M., Jr. (1990) *Chem. Rev. 90*, 585−606.

Lipscomb, J. D. (1994) *Annu. Rev. Microbiol. 48*, 371−399.

Liu, K. E., & Lippard, S. J. (1991) *J. Biol. Chem. 266*, 12836−12839.

Liu, K. E., Valentine, A. M., Wang, D., Huynh, B. H., Edmondson, D. E., Salifoglou, A., & Lippard, S. J. (1995a) *J. Am. Chem. Soc. 117*, 10174−10185.

Liu, Y., Nesheim, J. C., Lee, S.-K., & Lipscomb, J. D. (1995b) *J. Biol. Chem. 270*, 24662−24665.

Mason, J. R., & Cammack, R. (1992) *Annu. Rev. Microbiol. 46*, 277−305.

Matsudaira, P. (1987) *J. Biol. Chem. 262*, 10035−10038.

McClay, K., Streger, S. H., & Steffan, R. J. (1995) *App. Environ. Microbiol. 61*, 3479−3481.

McClay, K., Fox, B. G., & Steffan, R. J. (1996) *App. Environ. Microbiol. 62* (in press).

Muira, A., & Dalton, H. (1995) *Biosci. Biotech. Biochem. 59*, 853−859.

Münck, E., Debrunner, P. G., Tsibris, J. C. M., & Gunsalus, I. C. (1972) *Biochemistry 11*, 855−863.

Münck, E., Surerus, K. K., & Hendrich, M. P. (1993) *Methods Enzymol. 227*, 463−479.

Newman, L. M., & Wackett, L. P. (1995) *Biochemistry 34*, 14066−14076.

Nordlund, I., Powlowski, J., & Shingler, V. (1990) *J. Bacteriol. 172*, 6826−6833.

Olsen, R. H., Kukor, J. J., & Kaphammer, B. (1994) *J. Bacteriol. 176*, 3749−3756.

Paulsen, K. E., Liu, Y., Fox, B. G., Lipscomb, J. D., Münck, E., & Stankovich, M. T. (1994) *Biochemistry 33*, 713−722.

Petersson, L., Gräslund, A., Ehrenberg, A., Sjöberg, B.-M., & Reichard, P. (1980) *J. Biol. Chem. 255*, 6706−6712.

Powlowski, J., & Shingler, V. (1990) *J. Bacteriol. 172*, 6834−6840.

Rosenzweig, A. C., Frederick, C. A., Lippard, S. J., & Nordlund, P. (1993) *Nature 336*, 537−543.

Rosenzweig, A. C., Nordlund, P., Takahara, P. M., Frederick, C. A., & Lippard, S. J. (1995) *Chem. Biol. 2*, 409−418.
Saeki, H., & Furuhashi, K. (1994) *J. Ferm. Bioeng. 78*, 399−406.
Sands, R. H., & Dunham, W. R. (1975) *Q. Rev. Biophys. 7*, 443−504.
Schägger, H., & von Jagow, G. (1987) *Anal. Biochem. 166*, 368−379.
Shanklin, J., Whittle, E., & Fox, B. G. (1994) *Biochemistry 33*, 12787−12794.
Shields, M. S., Reagin, M. J., Gerger, R. R., Campbell, R., & Somerville, C. (1995) *App. Environ. Microbiol. 61*, 1352−1356.
Sjöberg, B.-M., Loehr, T. M., & Sanders-Loehr, J. (1982) *Biochemistry 21*, 96−102.
Stainthorpe, A. C., Lees, V., Salmond, G. P. C., Dalton, H., & Murrell, J. C. (1990) *Gene 91*, 27−34.
Suzuki, M., Hayakawa, T., Shaw, J. P., Rekik, M., & Harayama, S. (1991) *J. Bacteriol. 173*, 1690−1695.
Wackett, L. P. (1990) *Methods Enzymol. 188*, 39−45.
Whited, G. M., & Gibson, D. T. (1991) *J. Bacteriol. 173*, 3010−3016.
Wilson, K. (1993) *Preparation of Genomic DNA from Bacteria*, Current Protocols, Brooklyn, NY.
Yen, K.-M., & Karl, M. R. (1992) *J. Bacteriol. 174*, 7253−7261.
Yen, K.-M., Karl, M. R., Blatt, L. M., Simon, M. J., Winter, R. B., Fausset, P. R., Lu, H. S., Harcourt, A. A., & Chen, K. K. (1991) *J. Bacteriol. 173*, 5315−5327.
Zanetti, G., & Curti, B. (1980) *Methods Enzymol. 69*, 250−255.

BI960456M